ISSN: 2710-0588

Lithium Battery Health State Estimation Based on PSO-GPR Algorithm

Liguo Zhang[1], Zhipeng Zhu[1], Lingxi Zhang[2], Wenjie Zhao[1], Xingyu Ai[1]

[1]Northeast Petroleum University, Qinhuangdao 163319, China

[2]Yanshan University, Qinhuangdao 066000, China

Abstract

The State of Health (SOH) estimation of lithium-ion batteries is a critical factor in battery management systems, directly influencing performance evaluation and lifespan prediction. Traditional SOH estimation methods suffer from limitations such as insufficient accuracy and poor robustness, making it difficult to meet the demands of complex operating conditions. This paper proposes a novel SOH estimation method for lithium-ion batteries based on Particle Swarm Optimization (PSO) and Gaussian Process Regression (GPR). By analyzing the temperature variation curve during the constant-current charging process of lithium-ion batteries, three geometric features are extracted as health indicators. These features are combined with the peak information from the incremental capacity curve to construct a PSO-GPR model for SOH estimation. Experimental results demonstrate that the proposed method outperforms traditional GPR and Backpropagation (BP) neural network methods in terms of prediction accuracy and robustness. The SOH estimation error for most batteries is within 2%, effectively improving the estimation accuracy of lithium-ion battery SOH.

Keywords

Lithium-Ion Battery, State of Health, Temperature Variation Curve, Incremental Capacity Curve, Pso-Gpr Algorithm.

1. Introduction

With the global energy transition and rapid development of the electric vehicle industry, lithium-ion batteries—as the core power source for electric vehicles—play a pivotal role in determining vehicle safety and range performance. However, as battery usage cycles increase, aging becomes inevitable, manifesting as capacity degradation and elevated internal resistance, which adversely affect battery health status (State of Health, SOH). According to IEEE Standard 1188-1996, batteries require replacement when their capacity declines to 80% of initial capacity or internal resistance doubles from baseline levels. Therefore, accurate SOH estimation of lithium batteries is critical for ensuring safe operation and extending their service life.

Traditional State of Health (SOH) estimation methods primarily rely on the measurement and calculation of physical parameters such as voltage and current. Although simple to implement, these approaches overlook the nonlinear characteristics of batteries during charging and discharging processes, resulting in lower estimation accuracy[1]. In recent years, with the advancement of machine learning and data-driven methodologies, data-driven SOH estimation methods have emerged as a research hotspot[2]. Gaussian Process Regression (GPR), as a non-parametric Bayesian regression technique, effectively addresses nonlinear challenges and provides uncertainty measurements, demonstrating promising applications in SOH estimation[3]. However, the performance of GPR models heavily depends on hyperparameter selection, and traditional methods struggle to achieve global optimization of these

ISSN: 2710-0588

parameters[4]. Particle Swarm Optimization (PSO), as a global optimization algorithm, effectively avoids local optima and is well-suited for hyperparameter optimization in GPR models.

In the research on SOH estimation, Pearson Correlation Analysis, as a classical statistical analysis method, is commonly used to evaluate the correlation between different health factors and SOH. By calculating the correlation coefficients between various health factors and SOH, it is possible to effectively identify features with strong correlations to SOH, thereby improving the accuracy of SOH estimation models [5].

This study proposes a lithium battery State of Health (SOH) estimation method based on PSO-GPR. First, three geometric features are extracted from temperature variation curves during constant current charging to serve as health indicators. Second, the characterization capability of these health factors is enhanced by incorporating peak information from incremental capacity curves (ICC)[6]. Finally, the PSO algorithm optimizes GPR model hyperparameters to construct an SOH estimation framework. Experimental validation on the Oxford dataset demonstrates that our approach outperforms traditional GPR and BP neural network methods in both prediction accuracy and robustness, providing novel insights for precise SOH estimation in lithium batteries.

2. Battery Aging Data Analysis and Health Factor Extraction

2.1. Oxford University Battery Aging Dataset and Experimental Setup

This study utilized the battery aging dataset provided by the University of Oxford for experimental validation. The dataset comprises eight Kokam-brand lithium cobalt oxide pouch batteries (Cell1 to Cell8), each with a rated capacity of 740mAh[7]. Experiments were conducted at a constant ambient temperature of 40°C, employing a 2C (1.48A) constant current charging mode while simulating dynamic discharge processes under Artemis urban driving conditions to accelerate battery aging. After completing 100 charge-discharge cycles, battery capacity was calibrated through 1C constant current discharge to define a complete operational cycle. The dataset meticulously records capacity variation data for each battery throughout its lifecycle, providing a reliable foundation for state of health (SOH) prediction research. Figure 1 illustrates the capacity degradation trends of the eight batteries during aging processes.

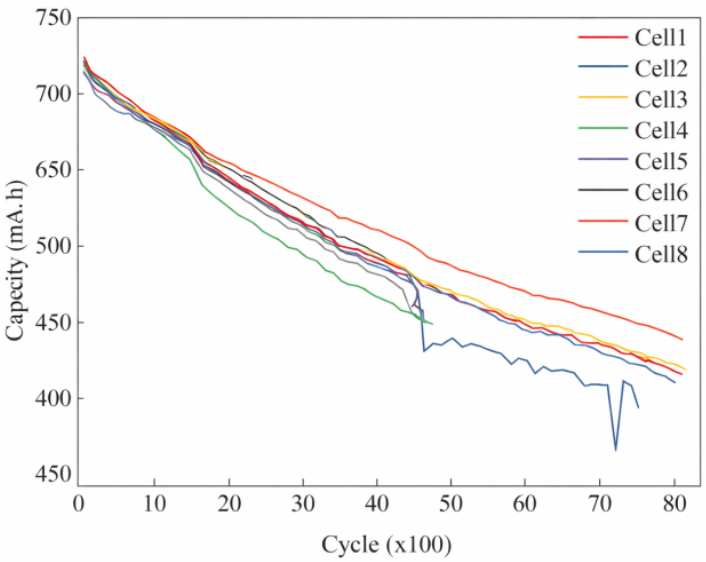

Figure 1. Capacity Degradation Curves of 8 Batteries in the Oxford Dataset

ISSN: 2710-0588

2.2. Temperature change rate curve acquisition

To mitigate the accuracy limitations of temperature sensors and external noise interference, direct calculation of temperature change rate may result in significant deviations. Accordingly, this study adopts the finite difference method for approximate computation of temperature change rate, as referenced in literature[8]. The finite difference method effectively reduces noise-induced effects on temperature change rate calculations, with the following computational formula:

$$DT(k) \approx \frac{T(k+L)-T(k)}{L} \tag{1}$$

In the formula, T denotes temperature and L represents the sampling interval. A larger step size L captures overall temperature variations across broader ranges, effectively reducing noise interference. However, excessively large L may fail to detect subtle fluctuations and rapid temperature changes. Conversely, a smaller L improves sensitivity to minute temperature variations but increases noise susceptibility, leading to unstable results and measurement errors. Based on temperature data availability, this study adopts L=40 as the sampling interval. The derived temperature rate curves are further smoothed using local weighted regression (LOESS) to minimize noise artifacts, ensuring more reliable and consistent temperature rate calculations.

Figure 2 presents partial DT curves of Cell1. The graph demonstrates that the battery temperature change rate (DT) initially exhibits a pattern of first decreasing and then increasing. During subsequent phases, the DT rate undergoes significant fluctuations, displaying distinct trends as the state of health (SOH) declines. As SOH decreases, the peak value on the left side of the DT curve gradually diminishes, while the central valley widens overall. Concurrently, the voltage difference between peaks and valleys (ΔV) progressively narrows. After reaching its peak following gradual ascent, the DT rate ultimately shows a downward trend. However, variations in DT curves remain relatively consistent across batteries with different SOH levels. Notably, DT curves exhibit a clear monotonic decline in their central region as SOH decreases—a trend of critical importance for understanding lithium battery aging mechanisms and SOH estimation. Accordingly, this study selects three health indicators: voltage V1 corresponding to the left-side peak of the DT curve, voltage V2 corresponding to the central valley, and the voltage difference ΔV between them. These parameters effectively capture temperature variation characteristics during battery aging processes, providing robust support for accurate SOH assessment.

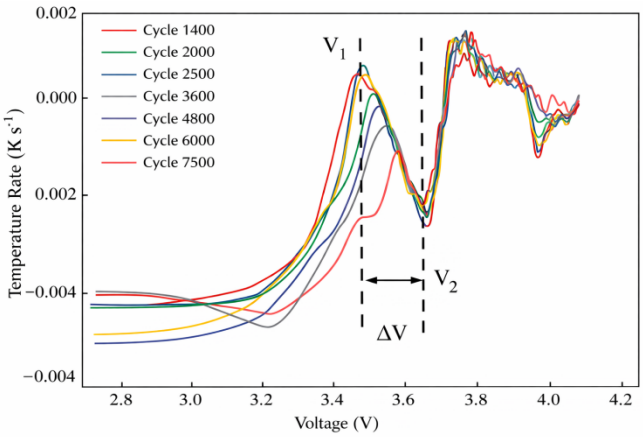

Figure 2. Partial DT Curves of Cell1

ISSN: 2710-0588

2.3. IC curve acquisition

IC analysis originated from Thompson's 1979 research in materials science[9]. With advancing studies, Dahn applied this method to carbon material research in lithium batteries during the 1990s[10]. In recent years, an increasing number of scholars have adopted IC analysis to investigate capacity fade mechanisms in lithium batteries. Mathematically, IC represents the additional energy stored in a battery across a continuous voltage increment range. Under constant current charging conditions, the IC calculation formula is:

$$IC = \frac{dQ}{dU} = I \cdot \frac{dt}{dU} \tag{2}$$

In the equation: Q represents capacity, U denotes voltage, and t stands for sampling time. Unlike traditional battery aging measurement methods (such as internal resistance and capacity decay assessment), IC analysis investigates battery aging mechanisms at the electrode level. One of its key advantages lies in converting battery voltage platforms into clearly identifiable peaks, thereby reflecting phase transition characteristics experienced during lithium-ion intercalation and deintercalation processes. Another critical strength of IC analysis is its real-time online capability, which provides unique advantages and potential in battery aging research. Taking Cell 1 from the Oxford dataset as an example, Figure 3 illustrates changes in IC curves during battery life evolution. As cycle counts increase, IC curves gradually flatten with significantly declining peak values (PICC), a trend that becomes more pronounced with repeated cycling. The distinctive shape, height, and position of IC curve peaks directly reflect electrochemical reaction characteristics during lithium battery charging and discharging processes[11]. According to literature[12–13], the reduction in PICC during charging data may correlate with active material loss in lithium batteries. With increasing cycle counts, active materials progressively lose their lithium-binding capacity, and these internal changes exert significant impacts on PICC values.

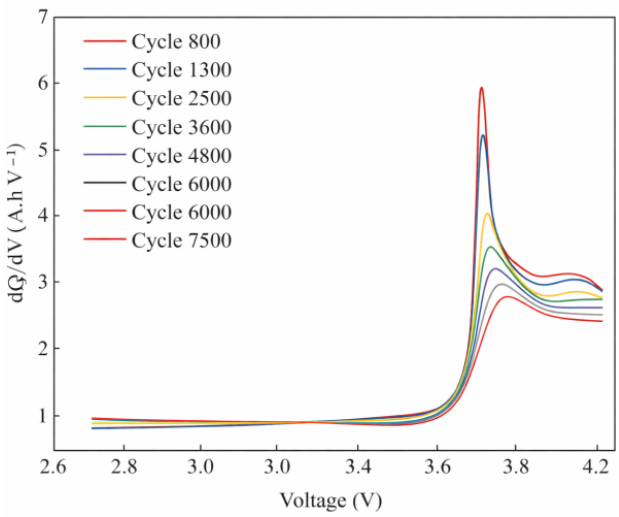

Figure 3. IC curve of Cell 1 under different cycles

Therefore, PICC is considered a key indicator for describing battery capacity degradation. Figure 4 presents the PICC curves of eight batteries from the Oxford Battery Dataset across different cycling cycles. As the number of cycles increases, the PICC values progressively decrease, reflecting the battery capacity degradation process and demonstrating a certain correlation with the battery's state of health (SOH).

ISSN: 2710-0588

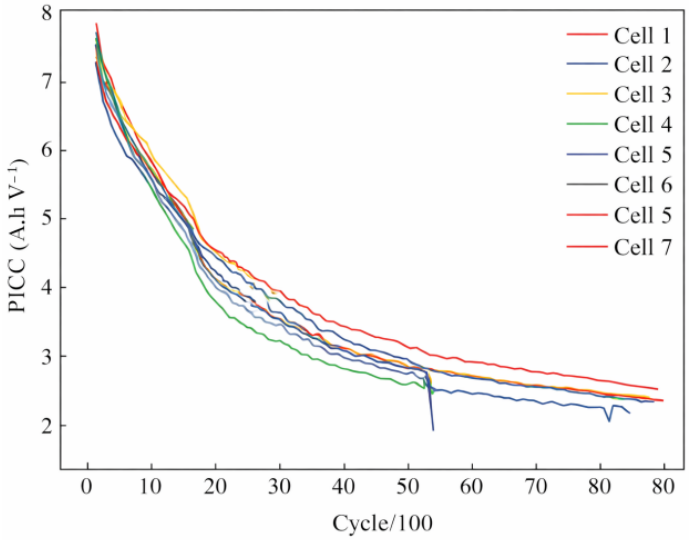

Figure 4. PICC curve

To date, this study has preliminarily identified four health characteristics reflecting changes in the state of health (SOH) of lithium-ion batteries. To further investigate the potential correlations between battery SOH and these health characteristics, Pearson correlation analysis was employed to evaluate the degree of association between the two variables [14]. The calculation formula for the Pearson correlation coefficient is as follows:

$$r = \frac{\sum_{i=1}^{n}(x_i - \bar{x})(y_i - \bar{y})}{\sqrt{\sum_{i=1}^{n}(x_i - \bar{x})^2}\sqrt{\sum_{i=1}^{n}(y_i - \bar{y})^2}} \tag{3}$$

In the formula, n denotes the sample size, xi and yi represent the selected features and the State of Health (SOH) of lithium batteries, respectively, while μ̄ denotes the sample mean. The correlation analysis results are presented in Table 1. Generally, a correlation coefficient |r|> 0.8 indicates strong correlation between variables, whereas |r| <0.5 suggests weak correlation. The table demonstrates that the selected features exhibit significant correlation with SOH

Table 1. Correlation analysis between different characteristics and battery SOH

cell	Voltage corresponding to the peak value	Voltage corresponding to the valley value	voltage difference	PICC
Cell1	-0.9868	0.8248	0.9541	0.9713
Cell2	-0.9413	0.8348	0.9836	0.9475
Cell3	-0.9399	0.8156	0.9678	0.9663
Cell4	-0.9898	0.8473	0.9881	0.9771
Cell5	-0.9781	0.8584	0.9933	0.9898
Cell6	-0.9879	0.8732	0.9932	0.9805
Cell7	-0.9714	0.8413	0.9902	0.9477
Cell8	-0.9929	0.8207	0.9930	0.9736

ISSN: 2710-0588

3. PSO-GPR Algorithm Theory

3.1. Gaussian Process Regression Theory

Unlike traditional regression methods, Gaussian Process Regression (GPR) does not require explicit specification of output forms. Instead, Gaussian processes treat the target values (y1, y2...yn) corresponding to an n-dimensional training set as n-dimensional sampling points within a Gaussian distribution[15]. Within this framework, there exists no simple one-to-one correspondence between the training set and corresponding target values. When constructing a Gaussian Process Regression model, Gaussian noise must be incorporated during data fitting, expressed as:

$$y = f(x) + N(0, \sigma_n^2) \tag{4}$$

the computation process, a Gaussian process prior is first applied to f(x), which can be expressed as:

$$f(x) \sim GP(0, K)\ f(x) \sim GP(0, K) \tag{5}$$

The covariance function can be expressed in the form of a squared exponential as:

$$k(x, x') = \sigma_f^2 \cdot \exp[-\frac{(x - x')^2}{2l^2}] \tag{6}$$

After considering noise, the above equation can be expressed

$$k(x, x') = \sigma_f^2 \cdot \exp[-\frac{(x - x')^2}{2l^2}] + \sigma_n^2 \cdot \delta(x, x') \tag{7}$$

In the formula, σf, σn, and l are optimal hyperparameters obtained through maximum likelihood estimation of the training set using a Gaussian process.

Next, we need to further derive the predicted value y* corresponding to the prediction set x*. This can be expressed as:

$$\begin{bmatrix} y \\ y^* \end{bmatrix} \sim N\left(0, \begin{bmatrix} K & K^{*T} \\ K^* & K^{**} \end{bmatrix}\right) \tag{8}$$

In the formula:

$$K = \begin{bmatrix} k(x_1, x_1) & k(x_1, x_2) & \cdots & k(x_1, x_n) \\ k(x_2, x_1) & k(x_2, x_2) & \cdots & k(x_2, x_n) \\ \vdots & \vdots & \ddots & \vdots \\ k(x_n, x_1) & k(x_n, x_2) & \dots & k(x_n, x_n) \end{bmatrix} \tag{9}$$

$$K^* = \begin{bmatrix} k(x^*, x_1) & k(x^*, x_2) & \cdots & k(x^*, x_n) \end{bmatrix} \tag{10}$$

ISSN: 2710-0588

$$K^{**} = k(x^*, x^*) \tag{11}$$

The above represents the expression for Gaussian process regression. To perform predictions using Gaussian process regression, Bayesian inference and joint density functions are employed for solving the prediction problem. The Bayesian formula is expressed as follows:

$$p(x \mid y) = \frac{p(y \mid x)p(x)}{p(y)} = \frac{p(y \mid x)p(x)}{\int p(y \mid x)p(x)dx} \tag{12}$$

The joint density function is expressed as:

$$p(x, y) = p(x \mid y)p(y) = p(y \mid x)p(x) \tag{13}$$

The Gaussian distribution is ultimately obtained as follows:

$$\overline{y^*} \mid y = N(K^* K^{-1} y, K^{**} - K^* K^{-1} K^{*T}) \tag{14}$$

Among $\overline{y^*} = K^* K^{-1} y$ $\overline{y^*} = K^* K^{-1} y$ them, the mean value can $\text{var}(y^*) = K^{**} - K^* K^{-1} K^{*T}$ be approximated as the $\text{var}(y^*) = K^{**} - K^* K^{-1} K^{*T}$ predicted value for the mean prediction; the variance represents the normal distribution of sample points.

3.2. Principle of PSO

After obtaining hyperparameters through maximum likelihood estimation of the training set, the PSO theory is applied to optimize these parameters to identify the optimal configuration. PSO (Particle Swarm Optimization) is an algorithm that iteratively searches for optimal solutions among randomly generated particles[16]. In an ionized particle swarm composed of m particles, each particle can be represented by an n-dimensional vector:

$$X_i = (x_{i1}, x_{i2}, \cdots, x_{in}), i = 1,2,\cdots,m \tag{15}$$

The velocity of particles can also be represented by an n-dimensional vector:

$$V_i = (v_{i1}, v_{i2}, \cdots, v_{in}), i = 1,2,\cdots,m \tag{16}$$

After establishing the position and velocity of particles in the particle swarm optimization (PSO) algorithm, the optimal positions of particles are iteratively searched and represented by an n-dimensional vector:

$$p_{best} = (p_{i1}, p_{i2}, \cdots, p_{in}), i = 1,2,\cdots,m \tag{17}$$

Through iterative optimization of each particle, the optimal position of the entire particle swarm is identified, represented by a vector:

$$g_{best} = (p_{g1}, p_{g2}, \cdots, p_{gn}) \tag{18}$$

ISSN: 2710-0588

The particle's position and velocity $i\ i$ are updated by identifying two optimal positions, with the following update method applied:

$$\begin{cases} v_{in}^{t} = \omega v_{in}^{t} + c_1 r_1 (p_{in} - x_{in}^{t}) + c_2 r_2 (p_{gn} - x_{in}^{t}) \\ x_{in}^{t+1} = x_{in}^{t} + v_{in}^{t+1} \\ (i = 1,2\cdots, m) \end{cases} \tag{19}$$

Here, ω denotes the inertia weight, t represents the iteration count, c1 and c2 are learning factors, while r1 and r2 are random numbers within the (0,1) interval.

3.3. Principle of PSO-GPR Algorithm

The core concept of the Particle Swarm Optimization-based Gaussian Process Regression (PSO-GPR) algorithm is to utilize the Particle Swarm Optimization (PSO) algorithm for hyperparameter optimization of Gaussian Process Regression (GPR) models, as illustrated in Figure 5.

As shown in Figure 5, the steps of the PSO-GPR algorithm[17] can be described as follows:

Input: The training set is defined as {(Xi, Yi)} with M_i=1, where Xi denotes the feature vector of the i-th training sample, Yi represents the regression value of the i-th training sample, and M indicates the total number of training samples. The independent evaluation dataset consists of {(Xeval_k, Yeval_k)} with Meval_k=1, where Xeval_k denotes the feature vector of the k-th evaluation sample, Yeval_k represents the regression value of the k-th evaluation sample, and Meval indicates the total number of evaluation samples. The parameters include: particle swarm size N, hyperparameter count m for Gaussian process regression (GPR), and maximum iteration limit T.

Output: Gaussian Process Regression Model (GPRfinal).

Step 1: Set the current iteration count j=0; initialize the particle swarm by randomly generating N particles denoted as p1, p2,..., pN. Each particle pi is assigned initial position

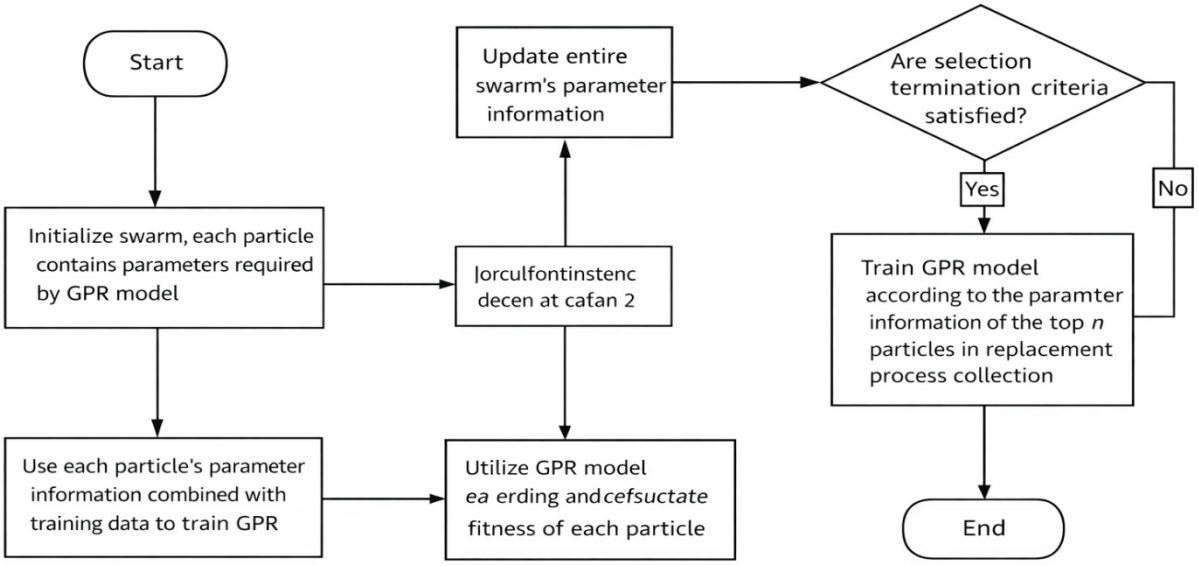

Figure 5. Flowchart of the PSO-GPR Algorithm

ISSN: 2710-0588

x(j)= {x(j)1, x(j)2,..., x(j)m} and velocity v(j) = {v(j)1, v(j)2,..., v(j)m}, where x(j)l represents the value of the l-th GPR hyperparameter at iteration j, and v(j)l denotes its corresponding increment during the same iteration.

Step 2: For each particle pi, extract GPR parameters based on its current position x(j)i, and train the GPR model on the training dataset, denoted as GPR(j)i.

Step 3: For each particle pi, evaluate the performance of its corresponding GPR (j) i using the Evaluation dataset, and calculate the fitness value f(x(j) i) according to the following formula.

$$f(x_i^{(j)}) = \frac{1}{M^{eval}} \sum_{k=1}^{M^{eval}} (Y_k^{eval} - GPR_i^{(j)}(X_k^{eval}))^2 \tag{20}$$

In the formula: GPR(j) i(Xeval k) denotes the predicted value of GPR(j) i for the evaluation sample Xeval k, while f(x(j) i) represents the root mean square error between the true values of samples in the evaluation dataset and their corresponding GPR(j) i predicted values.

Step 4: Determine the optimal positions pbest(j) for each particle pi and the global best position gbest(j) for the entire population during the first j iterations, based on equations (17) and (18).

Step 5: Update the position and velocity of each particle pi based on equations (15) and (16).

Step 6: If j=T, proceed to Step 7; otherwise, j=j+1 and return to Step 2.

Step 7: Extract optimal GPR parameters based on gbest(T), and then train the final prediction model GPRfinal on the training dataset.

4. Experimental Results and Analysis

The proposed PSO-GPR algorithm was validated for accuracy and effectiveness using eight battery datasets. Its superiority was further demonstrated through comparisons with traditional GPR algorithms and BP neural network algorithms commonly employed for predicting strong nonlinear relationships. The estimation results of the three algorithms are presented in Figure 6.

It can be observed that the PSO-GPR algorithm demonstrates superior accuracy compared to traditional GPR algorithms and BP neural network algorithms. The error performance of PSO-GPR on these eight battery datasets is illustrated in Figure 7, revealing that most batteries exhibit maximum errors below 2%. However, Cell2 batteries show significant deviations with peak errors reaching 11.21% and 9.87%, while Cell6 batteries demonstrate maximum errors up to 4.41%. Capacity degradation curves in Figure 1 indicate two instances of capacity collapse in Cell2 and one in Cell6, both of which substantially impact algorithm predictions. Potential causes of capacity collapse include operational variables during charge-discharge cycles (e.g., ambient temperature, voltage fluctuations, mechanical stress) or internal battery failures [8]. Comparative analysis of other batteries reveals PSO-GPR's enhanced accuracy and robustness. Table 2 presents key performance metrics for PSO-GPR's State of Health (SOH) estimation: Mean Absolute Error (MAE), Mean Absolute Percentage Error (MAPE), and Root Mean Square Error (RMSE). MAE quantifies error magnitude without directional bias, MAPE provides percentage-based accuracy evaluation, while RMSE measures convergence performance by reflecting the deviation between actual and estimated SOH states. These three evaluation criteria can comprehensively assess the SOH estimation error of the PSO-GPR algorithm.

ISSN: 2710-0588

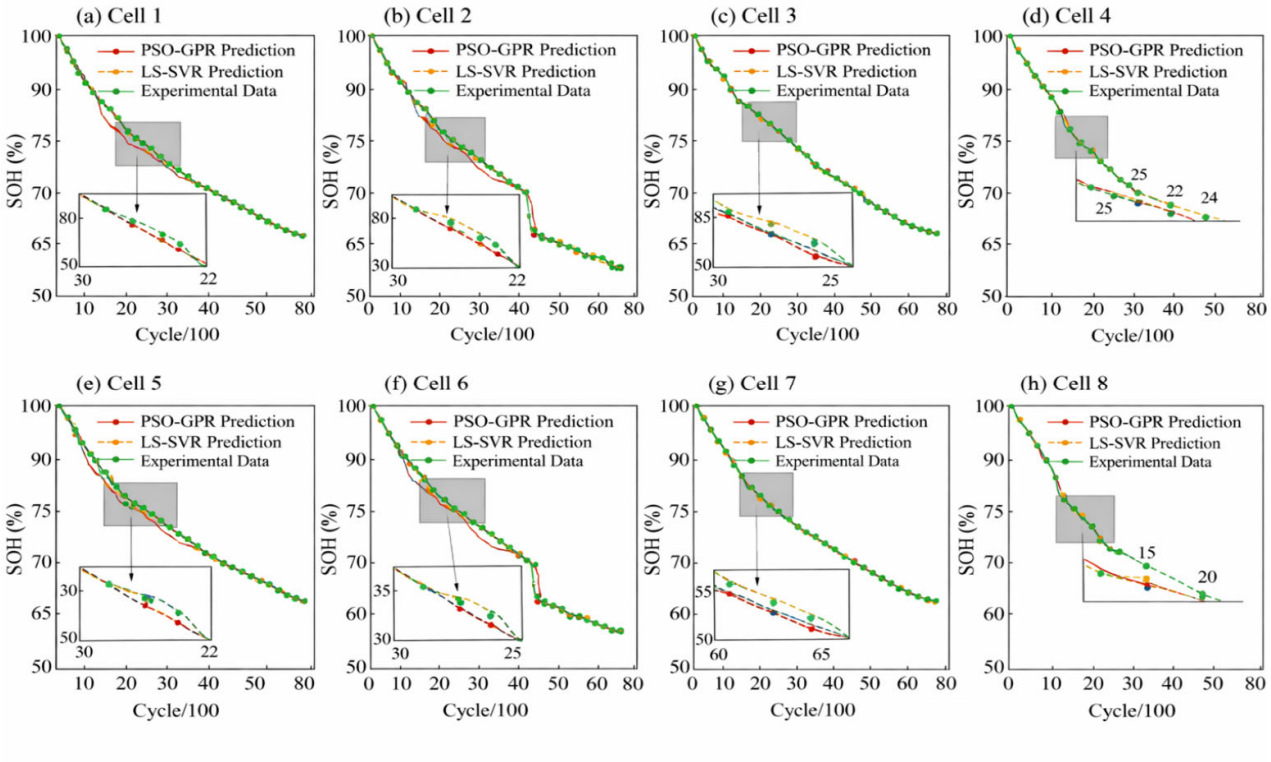

Figure 6. Comparison of True Values with Predictions from PSO-GPR, Traditional GPR, and BP Neural Network

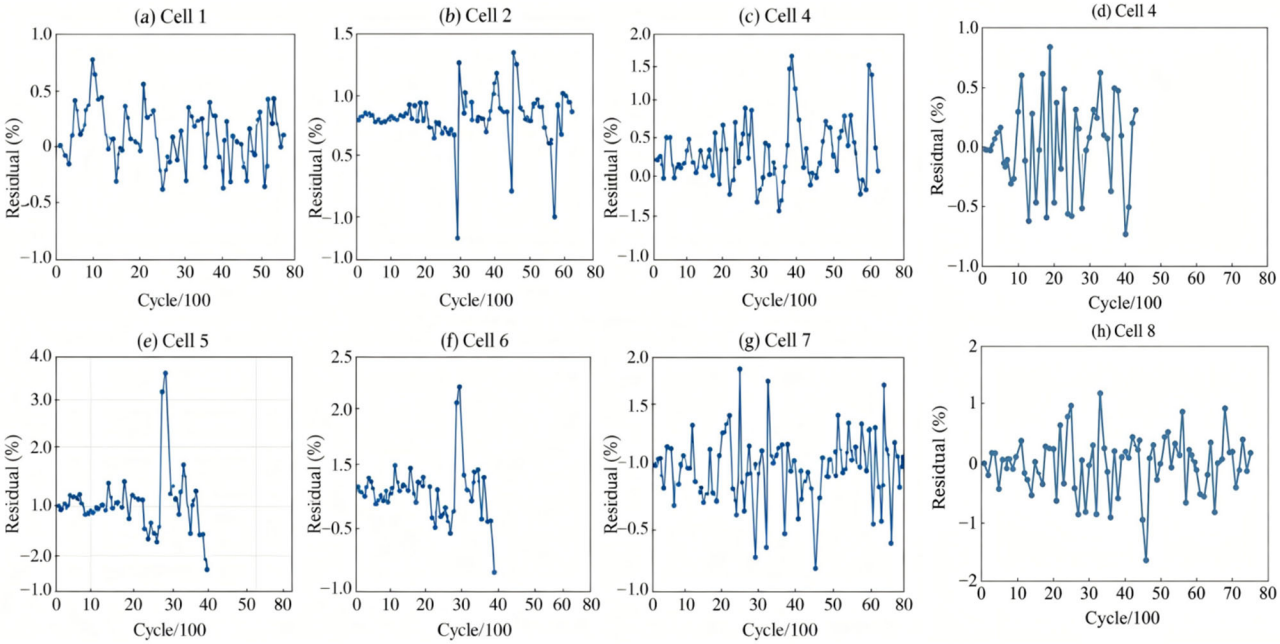

Figure 7. Error Analysis of the Battery Dataset

ISSN: 2710-0588

Table 2. Error Metrics of PSO-GPR Algorithm

cell	MAE	MAPE(%)	RMSE
Cell1	0.0013	0.18	0.0016
Cell2	0.0083	0.92	0.0092
Cell3	0.0028	0.39	0.0035
Cell4	0.0024	0.32	0.0029
Cell5	0.0028	0.36	0.0052
Cell6	0.0057	0.79	0.0081
Cell7	0.0021	0.28	0.0027
Cell8	0.0026	0.35	0.0033

This study proposes a lithium battery state of health (SOH) estimation method based on PSO-GPR algorithm. By analyzing temperature variation curves during constant current charging processes, three geometric features were extracted as health indicators. Combining peak information from incremental capacity curves (ICC), a PSO-GPR model was constructed for SOH estimation. Experimental results demonstrate that our method outperforms traditional GPR and BP neural network approaches in both prediction accuracy and robustness, with most batteries achieving SOH estimation errors below 2% and some reaching as low as 0.6%. The method effectively handles abnormal conditions such as sudden capacity drops, exhibiting strong robustness. This provides reliable technical support for lithium battery health management in electric vehicles and energy storage systems, significantly enhancing battery safety and longevity while reducing failure risks caused by aging. Future research will focus on optimizing health indicator extraction methods and exploring practical applications in battery management systems.

References

[1] Zhang Wei, Li Qiang, Wang Lei. A review of data-driven methods for lithium-ion battery state of health estimation[J]. Acta Automatica Sinica, 2021, 47(5): 1021-1035.

[2] Li X, Wang Z, Zhang J, et al. Data-driven methods for lithium-ion battery state of health estimation: A review[J]. Journal of Power Sources, 2021, 491: 229-245.

[3] Chen Y, Liu H, Zhang W, et al. Gaussian process regression for lithium-ion battery state of health estimation with uncertainty quantification[J]. IEEE Transactions on Industrial Informatics, 2022, 18(3): 1567-1578.

[4] Wang Peng, Li Na, Chen Xiaodong. Research on hyperparameter optimization of Gaussian process regression model based on particle swarm optimization algorithm[J]. Control and Decision, 2021, 36(8): 1897-1904.

[5] Zhu Dawei, Zhang Bo, Wang Fei, et al. State of health estimation method for lithium-ion batteries based on incremental capacity curve[J]. Application of Electronic Technique, 2019, 45(8): 118-123.

[6] Lin Mingqiang, Wu Denggao, Zheng Gengfeng, et al. State of health estimation for lithium-ion batteries based on surface temperature and incremental capacity[J]. Automotive Engineering, 2021, 43(09): 1285-1290+1284.

[7] Wang Ping, Gong Qingrui, Zhang Jiong, et al. An online state of health prediction method for lithium-ion batteries based on the combination of data-driven and empirical models[J]. Transactions of China Electrotechnical Society, 2021, 36(24): 12.

[8] TIAN J, XIONG R, SHEN W. State-of-health estimation based on differential temperature for lithium ion batteries [J]. IEEE Transactions on Power Electronics, 2020, 35 (10): 10363-10373.

[9] THOMPSON A H. Electrochemical potential spectroscopy: a new electrochemical measurement [J]. Journal of The Electrochemical Society, 1979, 126 (4): 608-616.

ISSN: 2710-0588

[10] GAO Y, DAHN J R. Synthesis and characterization of LiMnO for Li-ion battery applications [J]. Journal of The Electrochemical Society, 1996, 143 (1): 100-114.

[11] ANSEAN D, GARCIA V M, GONZALEZ M, et al. Lithium-ion battery degradation indicators via incremental capacity analysis [J]. IEEE Transactions on Industry Applications, 2019, 55: 2992–3002.

[12] BIRKL C , ROBERTS M R, McTURK E, et al. Degradation diagnostics for lithium ion cells [J]. Journal of Power Sources, 2017,341: 373-386.

[13] HAN X, LU L, ZHENG Y, et al. A review on the key issues of the lithium ion battery degradation among the whole life cycle [J].eTransportation, 2019, 1: 100005.

[14] PAN H, LU Z, WANG H, et al. Novel battery state-of-health online estimation method using multiple health indicators and an extreme learning machine [J]. Energy, 2018, 160: 466-477.

[15] Feng Chao, Jia Aoyin, Li Chentao, et al. Prediction of failure stress for defective pipelines based on PSO-GPR[J]. Mechanics in Engineering, 2023, 45(2): 260-266.

[16] Yin Xiaoye. Research on function optimization solving method based on particle swarm optimization algorithm[J]. Application of IC, 2022, 39(9): 210-211.

[17] Xu, B., Meng, X., Tian, A., Sun, Y., Cao, L., & Jiang, Y. (2022). State-of-charge prediction of lead-acid batteries based on particle swarm optimization and Gaussian process regression. Chinese Journal of Power Sources, *46*(8), 123-128.